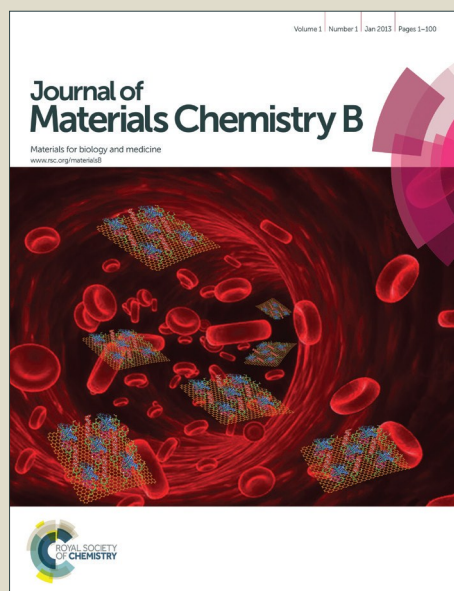


Journal of Materials Chemistry B

Accepted Manuscript



This is an *Accepted Manuscript*, which has been through the Royal Society of Chemistry peer review process and has been accepted for publication.

Accepted Manuscripts are published online shortly after acceptance, before technical editing, formatting and proof reading. Using this free service, authors can make their results available to the community, in citable form, before we publish the edited article. We will replace this *Accepted Manuscript* with the edited and formatted *Advance Article* as soon as it is available.

You can find more information about *Accepted Manuscripts* in the [Information for Authors](#).

Please note that technical editing may introduce minor changes to the text and/or graphics, which may alter content. The journal's standard [Terms & Conditions](#) and the [Ethical guidelines](#) still apply. In no event shall the Royal Society of Chemistry be held responsible for any errors or omissions in this *Accepted Manuscript* or any consequences arising from the use of any information it contains.

Cite this: DOI: 10.1039/c0xx00000x

www.rsc.org/xxxxxx

ARTICLE

Multifunctional REDV-conjugated zwitterionic polycarboxybetaine-polycaprolactone hybrid surfaces for enhanced antibacterial activity, anti-thrombogenicity and endothelial cell proliferation

Shaojun Yuan,^{a,*} Gordon Xiong,^b Fei He,^a Wei Jiang,^a Bin Liang,^a and Cleo Choong^{b,*}

Received (in XXX, XXX) Xth XXXXXXXXX 2015, Accepted Xth XXXXXXXXX 20XX

DOI: 10.1039/b000000x

The ideal synthetic polymeric vascular scaffolds should provide an excellent physiological environment to facilitate cell adhesion and growth, and the appropriate physicochemical properties to prevent thrombogenicity and secondary infection. In the current study, a multifunctional polycaprolactone (PCL) surface for simultaneously enhancing the adhesion and proliferation of endothelial cells (ECs), as well as inhibiting pathogenic microbial adhesion and preserving hemocompatibility was demonstrated. The achievement of such multifunctional surface was accomplished by the conjugation of Arg-Glu-Asp-Val (REDV) short peptides to zwitterionic polycarboxybetaine brushes-grafted PCL films via surface-initiated atom transfer radical polymerization (ATRP). *In vitro* antibacterial test demonstrated a high antibacterial efficiency against Gram-negative *E. coli* on the as-synthesized REDV-conjugated zwitterionic polycarboxybetaine hybrid surfaces. In addition, platelet adhesion assay results showed that the zwitterionic polycarboxybetaine-REDV conjugates led to the amelioration of surface hemocompatibility, and this enhancement was not negated by the conjugation of REDV. Cellular studies further revealed that the EC attachment and proliferation were substantially improved by zwitterionic polycarboxybetaine-REDV conjugation as compared to other PCL surfaces. The current multifunctional PCL hybrid surface is potentially useful in tissue engineered constructs for vascular graft applications as it allows for better initial attachment and proliferation of ECs, improved hemocompatibility, whilst simultaneously reducing graft-associated infections.

1. Introduction

The rising incidences of cardiovascular diseases worldwide have necessitated the development of vascular tissue replacements. While synthetic polymeric vascular grafts have the potential to overcome existing challenges posed by autologous vascular tissue grafts (e.g. the shortfall in demand or the lack of healthy vasculature in certain patients), the widespread clinical use of synthetic grafts has been limited by material thrombogenicity, which is mainly triggered by protein adsorption and platelet attachment or activation on graft surfaces.^{1, 2} One widely investigated approach to prevent thrombosis is the seeding of endothelial cells (ECs) onto the scaffold to prevent direct contact between the blood and synthetic material.³ Many studies have implicated delayed or absent stent endothelialization in late thrombosis and adverse clinical outcomes.⁴ Thus, the endothelialization of vascular grafts is an important step for preventing restenosis and ensuring long-term patency of the vascular grafts.³

While many studies have demonstrated good endothelial cytocompatibility or thromboresistance with functionalized surfaces, these studies do not concurrently address the issue of bacterial infections on functionalized surfaces.^{5, 6} In spite of the use of antibiotic prophylaxis, graft infections still occur in about 7% of vascular reconstruction procedures, and they constitute the most serious complication of such procedures with a high mortality rate.^{7, 8} Studies have also shown that synthetic grafts made from polytetrafluoroethylene (PTFE) and Dacron represent a higher risk of bacterial infection than autologous grafts. Therefore, an ideal vascular graft is a multifunctional graft that simultaneously integrates anti-thrombogenic and EC adhesive functionalities with antibacterial properties. Previous studies have demonstrated that multifunctional hybrid materials should provide the appropriate physicochemical and mechanical properties to prevent secondary infection, as well as excellent physiological environment to facilitate cell adhesion, proliferation and/or differentiation.^{9, 10} As surfaces with multiple functions often involve grafting of several different molecular moieties using different reactions, it is of great significance to develop a hybrid material with a multifunctional polymer conjugate instead.

^a Multiphase Mass Transfer & Reaction Engineering Lab, College of Chemical Engineering, Sichuan University, Chengdu, China 610065. Fax: 86 28 85460556; Tel: 86 28 85990133;

Email: yuanshaojun@gmail.com

^b Division of Materials Technology, School of Materials Science and Engineering, Nanyang Technological University, 50 Nanyang Avenue, 639798, Email: cleochoong@ntu.edu.sg

Electronic Supplementary Information (ESI) available: See DOI:10.1039/b000000x/

Biodegradable aliphatic polyesters have attracted attention in recent years for cardiovascular scaffolds materials, due to their good biocompatibility, nontoxicity, biodegradability, and controllable biodegradation rate.¹¹ Among them, polycaprolactone (PCL) has good mechanical strength and a degradation time of 2-4 years *in vivo*, making it a suitable non-permanent material affording ample time for the regeneration of new vascular tissue.¹² Different approaches have been developed to improve the hydrophilicity and cytocompatibility of PCL for improvement of cell adhesion and proliferation. Since PCL is lacking in reactive sites to allow for functional modification, specific functional polymer brushes containing pendant reactive hydroxyl (-OH), carboxyl (-COOH), amine (-NH₂) and epoxide groups have been successfully grafted onto the PCL surfaces using ozone treatment¹³, ultraviolet (UV) treatment¹⁴, plasma irradiation¹⁵, and irradiation-induced grafting¹⁶. However, these free radical polymerization techniques are associated with several limitations such as uncontrollable graft density or thickness of polymer brushes, undesired homopolymerization of monomers, as well as unfavorable reactions between reactive groups of polymer brushes and the material surface.¹⁷ On the contrary, surface-initiated polymerization (SIP) provides a well-controlled and highly efficient approach to control grafting density and thickness of polymer brushes by varying polymerization time and monomer concentrations.¹⁸ Among various SIP techniques, surface-initiated atom transfer radical polymerization (SI-ATRP), a newly-developed SIP technique to prepare functional polymer brushes of narrow polydispersity, precise architecture, controllable thickness and compositions, has gained increasing attention in surface functionalization of PCL scaffold materials for enhanced biocompatibility.¹⁹⁻²⁴

Zwitterionic polymers have been demonstrated to be highly resistant to non-specific protein adsorption and bacterial adhesion.^{25, 26} Some species of zwitterionic polymers have been evaluated for anti-thrombogenicity due to their resistance against platelet adhesion.^{27, 28} Accordingly, the main purpose of this study is to create a multifunctional surface of PCL scaffolds with antibacterial, blood-compatible and cytocompatible properties by the combination of grafting of zwitterionic polymers via SI-ATRP and covalent conjugation of short peptide Arg-Glu-Asp-Val (REDV). As schematically illustrated in Figure 1, the hydrophilic poly(dimethylaminopropyl methacrylamide) (PDMAPMA) brushes were first grafted onto the PCL film surface via surface-initiated ATRP of DMAPMA, followed by *N*-alkylation of the pendant tertiary amino groups on the side chains of the PDMAPMA brushes with sodium chloroacetate to generate zwitterionic polycarboxybetaine (QPDMAPMA) brushes. The carboxyl groups of the zwitterionic QPDMAPMA chains were capable of improving the hydrophilicity and resistance of nonspecific adsorption on the PCL scaffolds, while the quaternary ammonium compounds of QPDMAPMA chains endowed the surface with antibacterial activity. On the other hand,

the carboxyl groups on the zwitterionic QPDMAPMA chains also allowed for convenient immobilization of cell adhesive molecules via carbodiimide chemistry to promote EC attachment and growth. Short REDV peptides were immobilized onto the side chain of QPDMAPMA brushes to improve the EC cytocompatibility of the PCL scaffolds. REDV peptide was chosen because this short peptide sequence has been known to be selective for ECs.²⁹ REDV is specifically recognized by integrin $\alpha_4\beta_1$, which is expressed in abundance by ECs but not by other cell types such as mesenchymal stem cells (MSCs).³⁰ Our and other researchers' previous studies have demonstrated various strategies to functionalize polymer surfaces with the EC-specific adhesive peptide REDV to enhance EC attachment and proliferation.^{6, 31, 32} Each functionalization step was ascertained by attenuated total reflection-Fourier transform infrared spectroscopy (ATR-FTIR), X-ray photoelectron spectroscopy (XPS) and water contact angle measurements. The multifunctionality of functionalized PCL scaffolds was assessed by separate *in vitro* assays for anti-bacterial behavior, anti-platelet attachment and EC adhesion and proliferation.

2. Experimental

2.1 Materials

Polycaprolactone pellets (PCL, average Mn 45000), *N*-[3-(dimethylamino) 1,6-hexanediamine (98%), propyl] methacrylamide (DMAPMA, >98%), 2-bromoisobutyl bromide (BIBB, 98%), copper(I) bromide (CuBr, 99%), copper(II) bromide (CuBr₂, 98%), triethylamine (TEA, 98%), Sodium chloroacetate (ClCH₂COONa, 98%), *N,N,N,N*-pentamethyldiethylenetriamine (PMDETA, 98%), dichloromethane (anhydrous, >99.8%), 1-ethyl-3-(3-(dimethylamino) propyl) carbodiimide hydrochloride (EDC, 99%), and *N*-hydroxysuccinimide (NHS, 98%) were purchased from Sigma-Aldrich Chemical Co. (St. Louis, MO, USA). REDV short peptide was synthesized by ChinaPeptides Co. Ltd. (Shanghai, China), and were used without further purification. All the other chemical reagents and solvents were used as received. *E. Coli* (ATCC, 14948) was obtained from American Type Culture Collection (Manassas, VA, USA). Yeast extract, peptone, agar, and beef extract were purchased from Oxoid (Hampshire, UK). The Live/Dead Bac-Light bacterial viability kit L131152 was purchased from Life Technologies (Carlsbad, CA, USA). Human umbilical vein endothelial cells (HUVECs, ATCC CRL-1730) were obtained from the American Type Culture Collection (Manassas, VA). Cell culture medium (MCDB131), heparin, 4',6'-diamidino-2-phenylindole (DAPI), and paraformaldehyde (4%, w/v) were obtained from Sigma-Aldrich Chemical Co. Medium supplements, such as fetal bovine serum (FBS), Trypsin-EDTA (0.25%), bovine brain extract, amphotericin, penicillin, and streptomycin were purchased from Life Technologies. The alamarBlue (AB) assay and the LIVE/DEAD cell viability kit were also obtained from Life Technologies.

2.2. Grafting of PDMAPMA brushes via surface-initiated ATRP onto the PCL film surfaces

PCL films were prepared by an established solvent evaporation method in our previous study.³³ Detailed preparation procedures were described in the Supporting Information S1.1. The as-prepared PCL films were cut into round-shaped specimens with a diameter of 2 cm, and were washed with copious amounts of ethanol and deionized water. The clean PCL specimens were then activated by aminolysis treatment in a 10% (w/w) isopropanol solution of 1,6-hexanediamine at 40°C to introduce active amino groups using the previously-reported procedures,^{34, 35} as described in detail in Supporting Information S1.2. The resultant aminolyzed PCL films for 30 and 60 min were defined as the PCL-NH₂-1 and PCL-NH₂-2 surfaces, respectively. To immobilize the ATRP initiator through the reaction of the amino groups with 2-bromoisobutyl bromide (BIBB), the aminolyzed PCL films were immersed into 20 ml of dried hexane solution containing 1.5 mL of triethylamine (TEA) and 0.5 mL of BIBB. The reaction was allowed to proceed at 0°C for 2 h and then at room temperature for 24 h. The brominated PCL films from the PCL-NH₂-1 and PCL-NH₂-2 surfaces were referred to as the PCL-Br-1 and PCL-Br-2 surface, respectively. The PCL-Br surfaces were washed thoroughly with copious amounts of ethanol and deionized water prior to being dried under reduced pressure at room temperature overnight.

To graft PDMAPMA brushes from the PCL-Br surfaces, surface-initiated ATRP reaction was performed using a [DMAPMA]:[CuBr]:[CuBr₂]:[PMDETA] molar feed ratio of 100:1.0:0.2:2.0. An aliquot of 3 mL (17.50 mmol) of DMAPMA was introduced into a 25 mL round-bottom flask containing 5 ml of methanol/water mixture (5/1, v/v). The mixture was degassed with argon for 30 min prior to addition of 25.10 mg (0.175 mmol) CuBr, 7.82 mg (0.035 mmol) CuBr₂ and 73 μL (0.35 mmol) PMDETA. The reaction mixture was allowed to proceed at 35°C for 8 h. After the reaction, the resultant PDMAPMA-grafted PCL films were removed and rinsed with copious amount of methanol and deionized water to remove physically-adsorbed unreacted reactants prior to being dried under reduced pressure. The PDMAPMA-grafted PCL films from PCL-Br-1 and PCL-Br-2 surfaces were referred to as PCL-g-PDMAPMA1 and PCL-g-PDMAPMA2 surfaces, respectively.

2.3 Quaternization of PDMAPMA brushes and Conjugation of REDV peptide

The zwitterionic polycarboxybetaine brushes on the PCL film surfaces was achieved by *N*-alkylation of tertiary amino groups of the PDMAPMA chains with chloroacetate.³⁶ The PDMAPMA-grafted PCL films were immersed in a 30% aqueous solution of sodium chloroacetate, and the quaternization reaction was allowed to proceed at 50°C for 48 h. At the end of quaternization reaction, the resultant PCL films (defined as PCL-g-QDPMAPMA surfaces) were washed with copious amounts of ethanol and deionized water to remove the

physically-adsorbed reactants. Finally, the PCL-g-QDPMAPMA films were immersed in a 200 mL of 0.01 mol·L⁻¹ HCl solution for 12 h to remove the residual sodium before being dried under reduced pressure at 35 °C for 24 h.

The carboxyl groups (-COOH) on the zwitterionic QDPMAPMA brushes served as anchor sites to conjugate REDV short peptides via carbodiimide reaction. Typically, the zwitterionic PCL-g-QDPMAPMA films were pre-activated for 1 h at room temperature in a PBS solution (pH 7.4) containing 1 mg·mL⁻¹ NHS and 10 mg·mL⁻¹ EDC. Subsequently, the REDV short peptides were added to the above PBS solution at 3 mg·mL⁻¹ under continuous stirring. The reaction mixture was allowed to proceed at 25°C for 48 h to produce the PCL-g-QDPMAPMA-REDV surfaces. At the end of the conjugation reaction, the REDV-conjugated PCL films were washed with copious amounts of PBS and deionized water to remove the physically-adsorbed REDV peptides before being dried in vacuum oven at 25°C overnight.

2.4. Grafting density of PDMAPMA brushes and conjugated REDV peptides

The grafting density (GD) of PDMAPMA brushes and conjugated REDV peptides onto the PCL films were determined by the measurement of weight change per area before and after grafting using a previously-established procedure.³⁷ The grafting density (GD) was determined by the following equation:

$$GD = \frac{W_b - W_a}{A} \quad (1)$$

where W_a and W_b are the weights of the dry PCL film before and after grafting of PDMAPMA brushes, respectively, and A is the film area (about 3.2 cm²). For each GD measurement, at least three PCL films were investigated and the resulting values were averaged.

2.5 Surface density of carboxylic groups on the zwitterionic QDPMAPMA brushes

The surface concentration of carboxyl groups on the zwitterionic QDPMAPMA brushes was determined by a previously-established rhodamine-carboxyl interaction method.³⁸ Typically, an aliquot 4 mg of rhodamine 6G was dissolved in 4 mL of phosphate buffered solution (pH 12), and the solution mixture was immediately extracted with 100 ml of benzene with vigorous shaking. The extract showed an orange color and was used as the dye reagent for further experiments. The dye color could be changed from orange to pink in the presence of carboxyl compounds or polymers containing carboxyl groups. The appearance of the pink rhodamine-carboxyl complex was measured in a TU-1810 UV-Vis spectrophotometer (PERSEE, Beijing, China) at 536 nm. The predetermined concentrations of DMAPMA dissolved in the dye reagent were used to obtain a calibration curve of carboxyl groups. The QPMADMA-grafted PCL films were dissolved in DMF to obtain polymer solution. An equal volume of polymer solution (5 mL) and the rhodamine dye solution (5 mL) were mixed in a clean Pyrex test tube, followed by

standing for 10 min before being mounted on the spectrophotometer to measure the optical absorbance. The absorbance of bare PCL was measured as background control. The concentration of carboxylic groups in the solution was calculated from the standard calibration curve.

2.6 Surface characterization

The chemical compositions of surface-functionalized PCL films were determined by the ATR-FTIR and XPS characterization. The FTIR measurements were performed on a GX FTIR spectrometer (Perkin-Elmer Inc., Waltham, MA) equipped with a smart ATR performer accessory using a germanium (GE) with incident angle of 45° and a sampling area of 2 mm². The XPS spectra were collected on a Kratos AXIS Ultra^{DL} spectrometer with a monochromatic Al K α X-ray source (1486.6 eV photons), using procedures described in detail previously.³⁹ The surface wettability of the functionalized PCL films was determined by the measurement of static water contact angles. The static water contact angles were measured at 25 °C and 60% relative humidity using a sessile drop method with 5 μ l water droplets on a Powereach[®] JC2000C1 contact angle goniometer (Shanghai, China). The contact angles reported were the mean values from three samples, with the value of each substrate obtained by averaging the contact angles for at least three surface locations.

2.7 Determination of antibacterial activity of the functionalized PCL films

To determine the optimal solution pH for the PVBC-g-P Gram-negative *E.coli* was used as the bacterial strain to evaluate antibacterial capacity of the functionalized PCL films by visualization of attached bacterial colonies using the live/dead fluorescence method and an *in vitro* antibacterial test. Detailed procedures of bacterial cultivation were described in Supporting Information S1.3. The bacterial cell concentration in PBS suspension was chosen at 10⁷ cells·mL⁻¹ for the antibacterial assays. For the fluorescence antibacterial assays, the Live/Dead BacLight Bacterial Viability Kits, consisting of a mixture of SYTO 9 green fluorescent nucleic acid dye and propidium iodide (PI) red fluorescent nucleic acid dye, were used. The viability of bacterial cells upon contact with the functionalized PCL films can be distinguished from fluorescence color of the stained bacteria (green for viable cells and red for dead cells). Typically, each PCL film was immersed in 5 mL of the PBS bacterial suspension in a sterile Erlenmeyer flask. The flask was then shaken at 200 rpm at 37°C for 3 h. After the predetermined incubation time, the films were gently washed twice with PBS to remove the loosely-attached bacterial cells, and subsequently stained by dropping 0.1 mL solution of the BacLight Kits on the substrate surfaces for 15 min. The stained films were imaged under a green filter (excitation/emission, 420-480 nm/520-580 nm) or a red filter (excitation/emission, 480-550 nm/590-800 nm) with a Leica DMLM microscope, equipped with a 100 W Hg lamp. At least three different surface areas were

randomly chosen for FM imaging on each substratum to be representative of the entire surface.

In vitro antibacterial test was used to evaluate the antibacterial properties of the functionalized PCL films in a more quantitative manner. Briefly, the PCL films were separately placed in a 12-well plate, and 1 mL of bacterial suspension in PBS was pipetted onto the surface of each PCL film to ensure complete coverage of bacterial suspension. The well plates were placed in a 25 °C water bath to ensure a wet incubation atmosphere. At a predetermined time, an aliquot of 50 μ L bacterial suspension was collected from the PCL film surface with pipettes and serially diluted. 0.2 mL aliquots of the serially diluted suspension were plated onto solid agar using the spread plate method in triplicates. After incubation of the plates at 37 °C for 24 h, the number of viable cells (colonies) was counted manually and the results after multiplication with the dilution factor were expressed as the mean colony forming units (CFU) per mL. The survival ratio of bacterial cells was defined as the percentage of viable cells in the bacterial suspension in relative to the total number of the initial bacterial cells in the suspension.

2.8 Platelet adhesion array

Platelet-rich plasma (PRP) was obtained by centrifuging citrate anti-coagulated blood at 10,000 rpm for 15 min at room temperature. The PCL films were sterilized by immersion in a 70% ethanol for 2 h, followed by washing with copious amounts of sterile PBS solution, and then dried for 15 min in a biosafety cabinet. The PCL films were separately placed into a 6-well plate, and 5 mL of PRP was dispensed onto the surface of each PCL films. The well plates were incubated at 37°C under a 5% CO₂ atmosphere for 90 min. At the end of the incubation period, the PRP was carefully removed from the wells, and the PCL films were rinsed thrice with sterile PBS solution to remove any unattached platelet. The platelet-attached PCL films were then immersed into 2.5% glutaraldehyde solution at -4°C for 2 h for fixation, followed by stepwise dehydration with serial ethanol solutions from 25% to 100% for 5 min each. Finally, the platelet-attached PCL films were dried and sputter-coated with an ultrathin layer of platinum before being mounted on a JSM 5410LV SEM (JEOL, Tokyo, Japan) for SEM imaging. Five randomly-chosen locations of each film were imaged to obtain a statistical assessment of the quantity of the attached platelet.

2.9 Cell adhesion and proliferation assays

Human umbilical vein endothelial cells (HUVECs, ATCC CRL-1730TM) were used to assess the cytocompatibility of the functionalized PCL films. The cell culture procedures were described in detail in Supporting Information S1.4. Tissue culture polystyrene (TCPS) was used as the positive control for cell adhesion and proliferation. Prior to cell seeding, the pristine PCL and surface-functionalized PCL films were sterilized with 70% ethanol for 2 h, rinsed thrice with sterile PBS solution and

equilibrated in a culture medium for 2 h. For the cell adhesion assay, the PCL films were separately placed into a 12-well plate, and a 1.0 mL aliquot of HUVECs cell suspension (2×10^4 cells·mL⁻¹) was seeded onto the surface of pre-wetted PCL films in each well. The plates were then incubated under a 5% CO₂ atmosphere and 90% humidity at 37 °C for 24 h to allow for the cell attachment. At the end of incubation period, the cell-adhered PCL films were washed thrice with copious amount of sterile PBS solution to remove any unattached cells, and were then fixed with paraformaldehyde (4%, w/v) in PBS solution for 20 min at room temperature. A 200 μL aliquot of DAPI at 5 mg·mL⁻¹ in PBS was added to each surface of PCL films in the 12-well plate for 30 min at room temperature. The cells were then washed with sterile PBS solution and mounted between glass slides with glycerol. DAPI-stained fluorescence images of EC nuclei were captured under an excitation of 380 nm using a Nikon Image Ti fluorescence microscope and the NIS-Elements Br software (Nikon Instruments, Japan).

The AlamarBlue™ (AB) assay was used to determine cell viability and proliferation on the PCL films. A 1.0 ml aliquot of HUVECs cell suspension (2×10^4 cells/ml) was seeded onto the PCL films in each well of 12-well plate and incubated in a 5% CO₂ environment at 37 °C for 1, 3, 5 and 7 days. At the end of each incubation period, culture media was removed from the wells, and 0.5 ml of the AB solution (10% AB solution in culture media without FBS) was added to the wells. The plates were incubated in a 5% CO₂ atmosphere at 37°C for 4 h and the fluorescence intensity was measured using a microplate reader (Model 680, Bio-Rad Laboratories, Hercules, CA) at an excitation wavelength of 570 nm and an emission wavelength of 580 nm. Cell numbers were calculated using a standard curve correlating known cell numbers to fluorescence values. After each assay, the cells on the surfaces could be maintained in fresh medium after washing twice with sterile PBS, thus allowing continuous monitoring the cells on the same surface over the entire course of 7 days.

In vitro qualitative analysis of cell viability and coverage was performed using the LIVE/DEAD® Viability/Cytotoxicity Kit to assess the endothelialization extent on the PCL film surfaces. After 7 days of incubation, the culture medium was removed and each PCL film was washed thrice with sterile PBS solution. The working solution containing 2 mM Calcein-AM and 4 mM EthD-1 was then added directly to each PCL film. After incubation at room temperature for 45 min, the PCL films were observed using a Nikon Image Ti fluorescence microscope (emission at 515 nm and 635 nm). Fluorescence images of stained EC cells were collected using the NIS Elements Br software (Nikon Instruments, Japan) at five randomly-selected locations on each film surface.

2.10 Statistical analysis

All experiments were performed with four replicates and in at least three independent settings. Statistical analyses were carried out by one-way analysis of variance (ANOVA). A p-value of less than 0.05 was considered

statistically significant. The quantitative results were expressed as mean ± standard deviation (SD).

3. Results and discussion

As schematically illustrated in Fig. 1, the development of multifunctional REDV-conjugated zwitterionic polycarboxybetaine-PCL hybrid surfaces required a five-step reaction process: a) the activation of the PCL film surface by aminolysis reaction to introduce reactive amino groups, b) the immobilization of alkyl bromide ATRP initiator via TEA-catalyzed condensation reaction, c) the grafting of well-defined PDMAPMA brushes onto the PCL films via surface-initiated ATRP, d) the *N*-alkylation reaction between pendant tertiary amino groups on the PDMAPMA chains with chloroacetate to produce zwitterionic QPDMAPMA brushes, and e) the covalent conjugation of REDV short peptides to the terminal carboxyl groups of zwitterionic QPDMAPMA chains via carbodiimide chemistry. Each functionalization step was ascertained by ATR-FTIR, XPS and water contact angles.

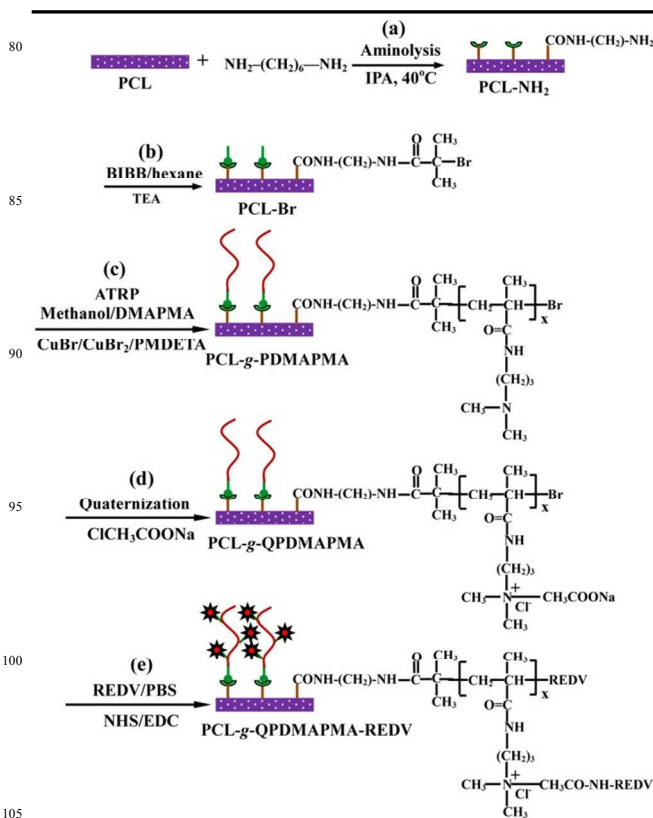


Fig. 1 Schematic illustration of the process of surface functionalization of PCL films: (a) aminolysis treatment of the PCL films to produce the PCL-NH₂ surface, (b) the immobilization of an alkyl-bromide containing ATRP initiator via TEA-catalyzed condensation reaction to generate the PCL-Br surface, (c) surface-initiated ATRP of DMAPMA to produce the PCL-g-PDAPMA surfaces, (d) the quaternization reaction of the PDAPMA brushes with sodium chloroacetate (ClCH₂COONa) to form zwitterionic polycarboxybetaine (the PCL-g-QPDAPMA surfaces), and (e) the covalent conjugation of REDV peptide onto the the QPDAPMA brushes via carbodiimide reaction to produce the PCL-g-QPDAPMA-REDV surfaces.

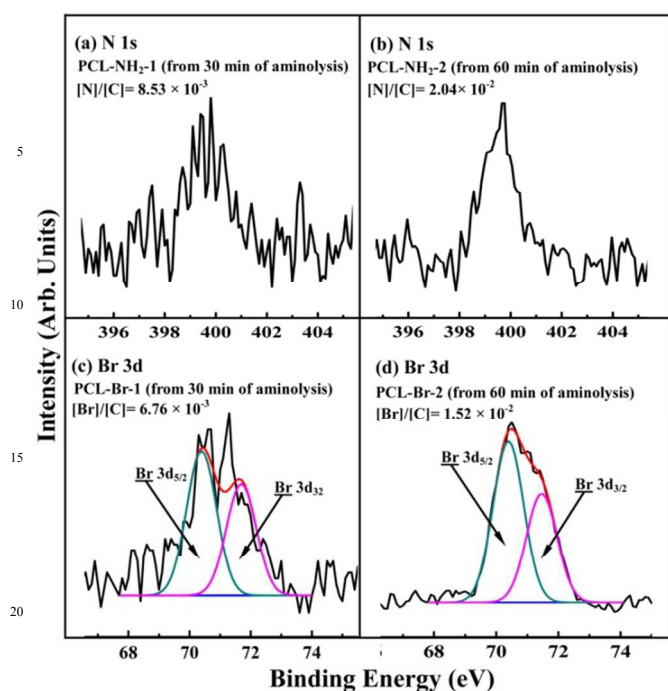


Fig. 2 XPS results showing N 1s and Br 3d core-level spectra of the (a) PCL-NH₂-1 (from 30 min of aminolysis), (b) PCL-Br-1 (from PCL-NH₂-1 surface), (c) PCL-NH₂-2 (from 60 min of aminolysis), and (d) PCL-Br-2 surfaces (from PCL-NH₂-2 surface).

3.1 Aminolysis treatment of PCL film and Immobilization of ATRP initiator

The grafting of reactive amino groups along the polyester chains was achieved by the aminolysis reaction between the ester groups (-COO⁻) of the PCL backbone and the terminal amine group of 1,6-hexanediamine.⁴⁰ The corresponding N 1s core-level spectra of the aminolyzed PCL film surfaces from 30 and 60 min were shown in Figs 2a and 2b, respectively. The [N]/[C] ratio, as determined from sensitivity factor-corrected N 1s and C 1s core-level XPS spectral areas, increases from 8.53×10^{-3} for the PCL-NH₂-1 surface (Fig. 2a) to 2.04×10^{-2} for the PCL-NH₂-2 surface (Fig. 2b). This result was well consistent with previous findings that the longer aminolysis reaction time can lead to higher surface density of amino groups on the PCL films surfaces.^{35, 41} The successful aminolysis of PCL films can be further deduced from the appearance of the three additional bands at 3434, 1640 and 1550 cm⁻¹, attributable to the stretching vibration of N-H (ν_{N-H}), amide I ($\nu_{C=O-NH}$) and amide II (δ_{N-H}) species, respectively (Supporting Information, Fig. S1).⁴² The results were consistent with the appearance of an additional N 1s signal with binding energy (BE) at 400 eV in the wide scan XPS spectra (Supporting Information, Figs. S2c and S2e) and an additional C-N peak component at 285.5 eV in the curve-fitted C 1s core-level XPS spectra (Figs. S2d and S2f),⁴³ as compared to those of the pristine PCL films (Figs. S2a and S2b). The presence of amino groups on the PCL-NH₂ surfaces was further confirmed by the decrease in static water contact angles of the PCL film surfaces from $96 \pm 3^\circ$

to $73 \pm 2^\circ$ (for the PCL-NH₂-1 surface) and $68 \pm 3^\circ$ (for the PCL-NH₂-2 surface) (Table 1). Hence, the reactive amino groups on the aminolyzed PCL film surface not only improved the surface hydrophilicity of inert PCL films, but also provided anchor sites to cater for further functionalization.

The immobilization of ATRP initiator onto the PCL films was accomplished by a TEA-catalyzed condensation reaction between the amino groups on the PCL-NH₂ surface and 2-bromoisobutyryl bromide (BIBB) (Fig. 1b). The appearance of three additional signals with BEs at 70, 189 and 256 eV, attributable to Br 3d, Br 3p and Br 3s species, respectively, in the wide scan XPS spectra suggested successful immobilization of an alkyl bromide-containing ATRP initiator with respect to those of the PCL-NH₂ surfaces. The corresponding Br 3d core-level spectra with a Br 3d_{5/2} at BE of 70.4 eV was consistent with the presence of alkyl bromine on the PCL-Br surface (Figs. 2c and 2d).⁴³ The surface ratios of [Br]/[C], as determined from the Br 3d and C 1s core-level spectral area, increased from 6.76×10^{-3} for the PCL-Br-1 (Fig. 2c) to 1.52×10^{-2} for the PCL-Br-2 surface (Fig. 2d), indicating that higher surface density of amino groups leads to the increase in surface density of ATRP initiator. The alkyl bromide initiator density was estimated to be about 1.5 initiators per nm² for the PCL-Br-1 surface and about 3.9 initiators per nm² for the PCL-Br-2 surface using a previously-established calculation method.⁴⁴ The successful immobilization of the alkyl bromide initiator on the PCL-Br surface was consistent with the evident increase in static water contact angle to $82 \pm 3^\circ$ for the PCL-Br-1 surface and $88 \pm 3^\circ$ for the PCL-Br-2 surfaces (Table 1).

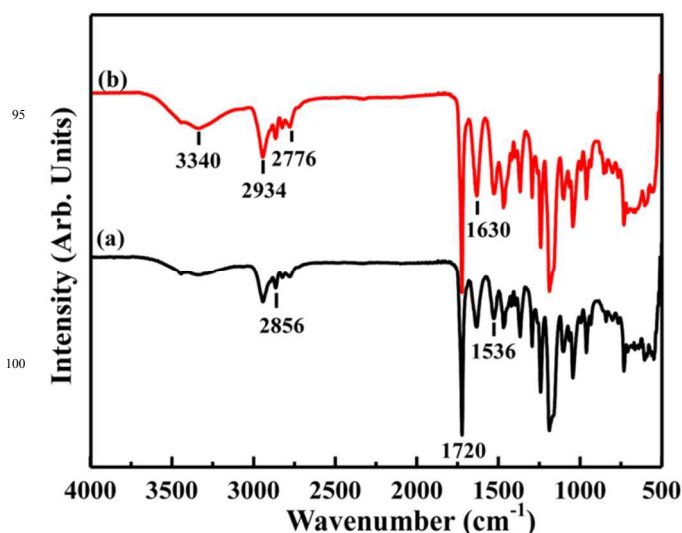


Fig. 3 ATR-FTIR spectra of the (a) PCL-g-PDMAPMA1 (from the PCL-Br-1 surface) and (b) PCL-g-PDMAPMA2 (from the PCL-Br-2 surface) surfaces after 8 h of ATRP reaction. Successful grafting of PDMAPMA brushes onto the PCL substrates was deduced from the characteristic bands at 3340 cm⁻¹ (ν_{N-H}), 2776 cm⁻¹ (ν_{C-H}) of N(CH₂) groups), 1630 cm⁻¹ (amide I) and 1536 cm⁻¹ (amide II).

Table 1. The grafting density, surface compositions, and water contact angles of the pristine PCL and functionalized PCL surfaces

| Sample | GD ^f (mg·cm ⁻²) (mean ± SD) | CCG ^g (μmol·cm ⁻²) | [Br]/[C] [N]/[C] ^h | WCA ⁱ (Degree) | WCA images |
|-------------------------------------|---|--|----------------------------------|------------------------------|--|
| PCL | – | – | – | 96 ± 3 |  |
| PCL-NH ₂ -1 ^a | – | – | 0.022 | 73 ± 2 |  |
| PCL-NH ₂ -2 ^a | – | – | 0.033 | 68 ± 3 |  |
| PCL-Br-1 ^b | – | – | 6.8×10 ⁻³ | 82 ± 3 |  |
| PCL-Br-2 ^b | – | – | 1.5×10 ⁻² | 88 ± 3 |  |
| PCL-g-PDMAPMA1 ^c | 1.30 ± 0.13 | – | 0.041 | 63 ± 3 |  |
| PCL-g-PDMAPMA2 ^c | 3.34 ± 0.17 | – | 0.11 | 58 ± 3 |  |
| PCL-g-QPDMAPMA1 ^d | 0.82 ± 0.03 | 2.02 ± 0.12 | 0.034 | 45 ± 3 |  |
| PCL-g-QPDMAPMA2 ^d | 1.95 ± 0.11 | 5.18 ± 0.20 | 0.051 | 34 ± 2 |  |
| PCL-g-QPDMAPMA1-REDV ^e | 0.82 ± 0.13 | – | 0.075 | 33 ± 2 |  |
| PCL-g-QPDMAPMA2-REDV ^e | 1.43 ± 0.17 | – | 0.11 | 24 ± 3 |  |

^a PCL-NH₂-1 and PCL-NH₂-2 surfaces were obtained by immersing the PCL films in a 10% (v : v) 1,6-hexanediamine/2-propanol solution for 30 and 60 min at 40°C, respectively. ^b PCL-Br-1 and PCL-Br-2 surfaces were obtained from the PCL-NH₂-1 and PCL-NH₂-2 surfaces, respectively, after 24 h of reaction with 2-bromoisobutyryl bromide (BIBB) in dried hexane containing 1 : 1 (molar ratio) BIBB and triethylamine (TEA). ^c Reaction conditions: [DMAPMA]:[CuBr]:[CuBr₂]:[PMDETA] = 100:1:0.2:2 in a mixture aqueous solution of methanol and deionized water (molar ratio 5:1) at 35°C for 8h. ^d Reaction conditions: the quaternization of the pendant tertiary amino groups of the corresponding PCL-g-PDMAPMA surfaces was performed in a 30% sodium chloroacetate solution (ClCH₂COONa) at 50°C for 48 h. ^e Reaction conditions: the corresponding PCL-g-QPDMAPMA surfaces were incubated in a PBS buffer (pH 7.4) containing 10:1 (molar ratio) EDC and NHS at 25°C for 1 h, and were subsequently transferred into a PBS solution containing REDV peptide at a concentration of 3 mg/ml at 25°C for 48 h. ^f Grafting density (GD) is defined as GD = (W_b - W_a)/A where W_a and W_b correspond to the weight of the dry films before and after grafting of polymer brushes, respectively, and A is the film area (about 1 cm²). SD denotes standard deviation. ^g CCG denotes the concentration of carboxyl groups on the QPDMAPMA brushes, which was determined by the rhodamine-carboxyl interaction method. ^h Determined from the corresponding sensitivity factor-corrected C 1s, N 1s and Br 3d core-level spectral area ratios. ⁱ WCA correspond to the static water contact angles.

3.2 Grafting of PDMAPMA brushes via surface-initiated ATRP

The surface-initiated polymerization of PDMAPMA chains took place for 8 h from the PCL-Br surfaces to produce the PCL-g-PDMAPMA surfaces (Fig. 1c). Fig. 3 showed the FTIR spectra of the PCL-g-PDMAPMA1 (from the PCL-Br-1 surface) and PCL-g-PDMAPMA2 surfaces (from the PCL-Br-2 surface), respectively. In comparison with the FTIR spectra of the PCL-Br surface, the appearance of three additional bands of the N-H stretching vibration (ν_{N-H}) at 3340 cm⁻¹, the stretching vibration amide I (ν_{C=O-NH}) at 1630 cm⁻¹ and the bending vibration amide II (δ_{N-H}) indicated the successful grafting of PDMAPMA brushes onto the PCL-g-PDMAPMA surfaces.⁴⁵ The relative intensity of the characteristic amide I, amide II and N-H peaks for the PCL-g-PDMAPMA2 surface were much stronger than that of the PCL-g-PDMAPMA1 surface, indicative of a positive correlation of the surface density of initiator with the grafting density of PDMAPMA brushes.

The XPS spectra of the PCL surfaces were used to further confirm the grafting of PDMAPMA brushes onto the PCL-g-PDMAPMA surfaces (Fig. 4). The successful grafting of PDMAPMA brushes onto the PCL surfaces can be deduced from the appearance of an additional N 1s signal and the disappearance of the Br signals in the wide scan XPS spectra of the PCL-g-PDMAPMA surfaces (Figs. 4a and 4d), as compared to those of the PCL-Br surfaces (Supporting Information, Figs. S3a and S3c). The [N]/[C] ratios, as determined from the N 1s and C 1s core-level spectral area, were approximately 0.094 for the PCL-g-PDMAPMA1 and about 0.154 for PCL-g-PDMAPMA2 surfaces. This result further confirmed that the grafting density of the polymer brushes was mainly dependent on the surface density of initiator sites. The curve-fitted C 1s core-level spectra of the PCL-g-PDMAPMA surface consisted of four peak components with BEs at 284.6, 285.5, 287.8 eV, and 288.6 eV, attributable to C-H, C-N, O=C-NH and O=C-O species, respectively (Figs. 4b and 4e).⁴³ The additional characteristic O=C-NH species and the increase in relative intensity of C-N species were both

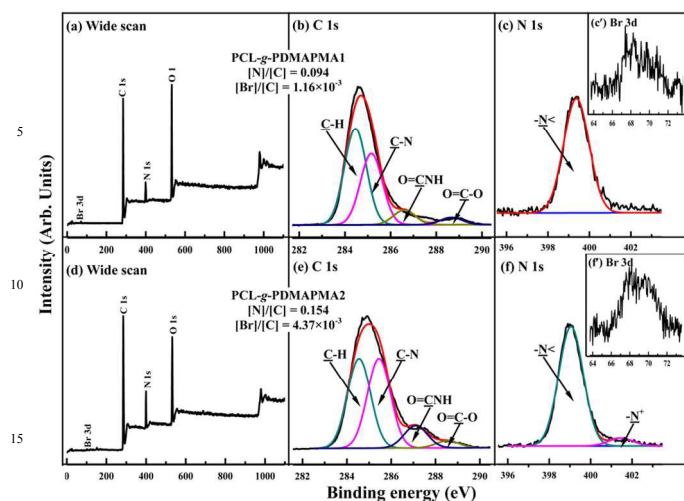


Fig. 4 Wide scan, C 1s, N 1s and Br 3d core-level XPS spectra of the (a,b,c,c') PCL-g-PDMAPMA1 (from the PCL-Br-1 surface) and (d,e,f,f') PCL-g-PDMAPMA1 (from the PCL-Br-1 surface) surfaces after 8 h of ATRP reaction. The appearance of additional N 1s signal indicated the successful grafting of PDMAEMA brushes on the PCL substrates.

consistent with the presence of PDMAPMA brushes on the PCL film surfaces. The predominant peak component at 399.3 eV of the curve-fitted N 1s core-level spectra was attributable to the neutral tertiary amine nitrogen ($-N<$) of the PDMAPMA chains (Figs. 4c and 4f). The minor peak component with BE at 401.8 eV, attributable to positively-charged nitrogen ($-N^+$), was ascribed to a small degree (around 3.2%) of self-quaternization of the PDMAPMA brushes by the terminal alkyl bromide groups from ATRP process (Fig. 4f).⁴⁶ The persistence of Br species (Br 3d_{5/2} and Br 3d_{3/2} doublet, Inset Figs. 4c' and 4f') was consistent with the previous findings that the “living” chain end from the ATRP reaction retain a dormant alkyl halide group, which was readily re-activated to initiate block copolymerization.⁴⁷ The surface wettability of the PDMAPMA-grafted PCL films became more hydrophilic with the decrease in static water contact angle to $63 \pm 3^\circ$ for the PCL-g-PDMAPMA1 surface and $58 \pm 3^\circ$ for the PCL-g-PDMAPMA2 surface (Table 1).

The growth kinetics of the PDMAPMA chains on the PCL film surfaces were determined by the measurement of the grafting density as a function of ATRP time (Supporting Information, Fig. S4). The grafting of PDMAPMA chains was found to occur in a time-dependent manner, since an approximate linear increase in the grafting density of the PDMAPMA chains was observed for both the PCL-g-PDMAPMA1 and PCL-g-PDMAPMA2 surfaces. However, the grafting density values of the PCL-g-PDMAPMA2 surface were much larger than those of the PCL-g-PDMAPMA1 surface, indicating that a higher surface density of initiator sites led to the increase in grafting density of polymer chains, and thus a more complete coverage of PDMAPMA brushes. The grafting density values of the PDMAPMA brushes from the PCL film surface with different surface densities

of initiators were about 1.30 ± 0.13 and 3.34 ± 0.17 $\text{mg}\cdot\text{cm}^{-2}$ for the PCL-g-PDMAPMA1 and PCL-g-PDMAPMA2 surfaces, respectively. These results were consistent with the previous findings that the surface density of initiator sites played a crucial role in determining the number of growing polymer chains and the grafting density of polymer brushes.^{20, 48}

3.3 N-alkylation to produce zwitterionic QPDMAPMA brushes

In this study, the zwitterionic polycarboxybetaine brushes were produced by the quaternization of pendant tertiary amino groups of PDMAPMA chains with sodium chloroacetate. Success in N-alkylation of PDMAPMA brushes was ascertained by FTIR and XPS characterization. The significant increase in the relative intensity of the characteristic bands at 3336 cm^{-1} ($\nu_{\text{O-H}}$), 1628 cm^{-1} (amide I, $\nu_{\text{C=O-NH}}$) and 1528 cm^{-1} (amide II, $\delta_{\text{N-H}}$) indicated that the tertiary amine groups in the side chains of the PDMAPMA brushes was quaternized to generate zwitterionic polycarboxybetaine brushes (QPDMAPMA) (Supporting Information, Fig. S5)⁴⁹. Fig. 5 showed the wide scan, C 1s, N 1s and Cl 2p core-level XPS spectra of the PCL-g-QPDMAPMA1 and PCL-g-QPDMAPMA2 surface, respectively. The appearance of additional Cl 2p (BE at 197 eV) and Cl 2s (BE at 230 eV) signals in the wide scan spectra indicated successful N-alkylation of the pendant tertiary amino groups on the PDMAPMA chains by sodium chloroacetate (Figs. 5a and 5d).⁴³ The C 1s core-level spectra of the PCL-g-QPDMAPMA surfaces can be curve-fitted into four peak components with BEs at 284.6, 285.5, 286.2, and 288.6 eV, attributable to C-H, C-N, C-N⁺/C-Cl and O=C-O species, respectively (Figs. 5b and 5e).

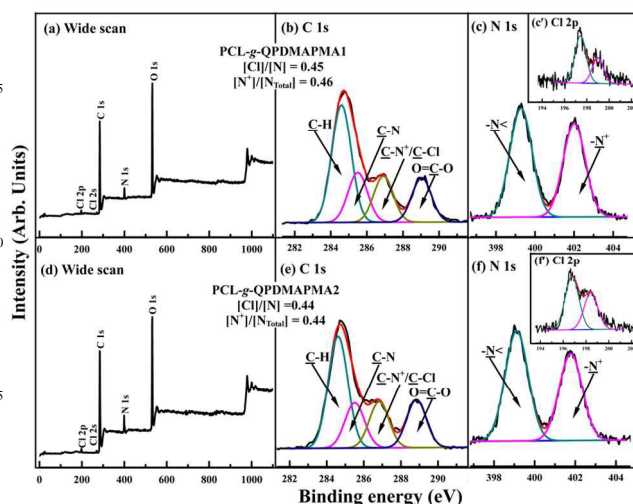


Fig. 5 Wide scan, C 1s, N 1s and Cl 2p core-level XPS spectra of the (a-c') PCL-g-QPDMAPMA1 (from the PCL-g-PDMAPMA1) and (d-f') PCL-g-QPDMAPMA2 (from the PCL-g-PDMAPMA2) surfaces. Successful N-alkylation of tertiary amino groups of the PDMAPMA brushes with $\text{ClCH}_2\text{COONa}$ was ascertained by the appearance of an additional Cl 2p signal in wide scan spectra and the peak component of positively-charged nitrogen ($-N^+$, with BE at 402.2 eV) in the curve-fitted N 1s core-level spectra.

In comparison with the curve-fitted C 1s spectra of the PCL-g-PDMAPMA surfaces (Figs. 4b and 4e), the disappearance of characteristic O=CNH species, the appearance of additional C-N⁺/C-Cl species, and the significant increase in the relative intensity of O=C-O species were consistent with the successful *N*-alkylation of tertiary amino groups in side chains of the PDMAPMA brushes. The corresponding curve-fitted N 1s core-level spectra of the PCL-g-QPDMAPMA surfaces consisted of two peak components with BEs at about 399.8 and 402.5 eV, attributable to the neutral (-N-) and the positively charged nitrogen (-N⁺), respectively (Figs. 5c and 5f). The [N⁺]/[N_{Total}] ratio, as determined from the spectral area of the two peak components, were calculated to be around 0.46 for the PCL-g-QPDMAPMA1 and 0.44 for the PCL-g-QPDMAPMA2 surfaces, indicating that nearly half of tertiary amino groups have been quaternized by sodium chloroacetate. Along with the quaternization reaction, the carboxyl groups were concurrently introduced to the PDMAPMA brushes to produce the zwitterionic QPDMAPMA brushes. Based on a well-established colorimetric method, the surface densities of the carboxyl groups on the PCL-g-QPDMAPMA1 and PCL-g-QPDMAPMA2 were determined to be about 2.02 ± 0.12 and 5.18 ± 0.2 μmol·cm⁻², respectively (Table 1). The presence of zwitterionic polycarboxybetaine (i.e. QPDMAPMA) brushes resulted in a more hydrophilic surface than pristine PCL films, as the static water contact angles on the PCL-g-QPDMAPMA1 and PCL-g-QPDMAPMA2 surfaces decreased to about 45 ± 3° and 34 ± 2°, respectively (Table 1).

3.4 Covalent conjugation of REDV peptides onto the zwitterionic QPDMAPMA chains

The abundant carboxyl groups in the side chains of QPDMAPMA brushes provide versatile anchor sites for

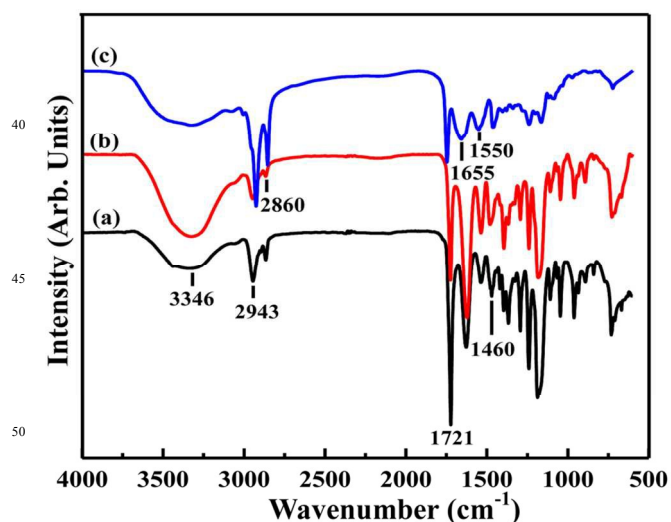


Fig. 6 ATR-FTIR spectra of (a) the PCL-g-PDMAPMA1-REDV surface, (b) the PCL-g-PDMAPMA2-REDV surface, and (c) pure REDV peptide. The characteristic bands at 3346 cm⁻¹ ($\nu_{(N-H)}$), 1655 cm⁻¹ (amide I) and 1550 cm⁻¹ (amide II) indicated the presence of REDV peptide on the PCL surfaces.

the immobilization of biologically-active molecules. As a fibronectin-derived peptide, REDV peptide has been known to selectively bind to ECs as the REDV short sequence is one of the main recognition sites for integrin $\alpha_4\beta_1$ receptors on the EC surface. This leads to specific interactions between fibronectin and ECs.³⁰ To covalently conjugate the REDV peptides onto the zwitterionic QPDMAPMA-grafted PCL films, the preactivation of carboxyl groups on the zwitterionic polycarboxybetaine chains was performed by EDC/NHS chemistry to introduce reactive esters (succinimidyl intermediates) on the QPDMAPMA-grafted surface.⁵⁰ The nucleophilic substitution reaction between the active esters and the amine groups of REDV peptides eventually resulted in a stable amide linkage (O=CNH) between REDV and zwitterionic QPDMAPMA brushes. As shown in Fig. 6, the main characteristic bands of the pure REDV peptide included a broad band of overlapping O-H/N-H stretching vibration in the wavenumber range of 3250 – 3600 cm⁻¹ (ν_{O-H} at about 3400 cm⁻¹ and ν_{N-H} at about 3250 cm⁻¹), amide I ($\nu_{C=ONH}$) at 1655 cm⁻¹ and amide II (δ_{N-H}) at 1550 cm⁻¹, respectively (Fig. 6c). As compared to the FTIR spectra of the PCL-g-QPDMAPMA surface (Figures S5), the broadening of the $\nu_{O-H/N-H}$ band, the increase in relative intensity of characteristic amide I peak, and the slight positive shifts of amide I ($\nu_{C=ONH}$) and amide II (δ_{N-H}) peaks suggested successful immobilization of REDV peptides onto the QPDMAPMA chains (Figs. 6a and 6b). The amide I ($\nu_{C=ONH}$) peak was associated with the peptide bonds in REDV and linkages formed between the -COOH of zwitterionic QPDMAPMA and the -NH₂ of the REDV molecules.

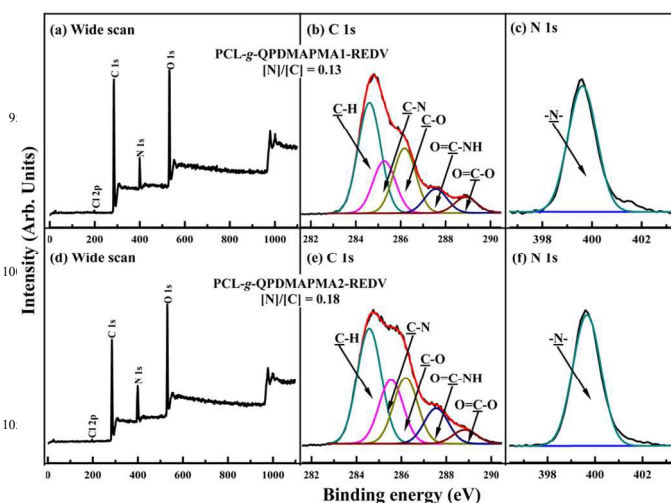


Fig. 7 Wide scan, C 1s and N 1s core-level XPS spectra of the (a,b,c) PCL-g-QPDMAPMA1-REDV and (d,e,f) PCL-g-QPDMAPMA2-REDV surfaces. The increase in relative abundance of N 1s signal in the wide scan spectra and the appearance of additional peak component of O=CNH (with BE at 278.8 eV) in the curve-fitted C 1s core-level spectra implied the successful conjugation of REDV peptide onto the carboxyl groups (-COOH) of the QPDMAPMA brushes.

The chemical composition of the REDV-conjugated zwitterionic QPDMA-PMA surface was also characterized by XPS measurement. Fig. 7 showed the respective wide scan, C 1s and N 1s core-level spectra of the PCL-g-QPDMA-PMA1-REDV and PCL-g-QPDMA-PMA2-REDV. The significant increase in the relative intensity of N 1s signal in the wide scan spectra was indicative of the successful immobilization of REDV peptides onto the zwitterionic QPDMA-PMA chains (Figs. 7a and 7d). The curve-fitted C 1s core-level spectra for the REDV-immobilized surfaces consisted of five peak components with BEs at 284.6, 285.5, 286.2, 287.8 and 288.6 eV, attributable to the C-H, C-N, C-O, O=C-NH and O=C-O species, respectively (Figs. 7b and 7e).⁴³ The characteristic O=C-NH species was attributed to the linkages in REDV peptide itself, as well as the linkage between QPDMA-PMA and REDV peptide. The only peak component with BE at 399.8 eV within the curve-fitted N 1s core-level spectra, attributable to neutral amino groups (-N-), was consistent with the successful immobilization of REDV peptide onto the zwitterionic QPDMA-PMA chains (Figs. 7c and 7f). The [N]/[C] ratios, as determined from the N 1s and C 1s core-level spectral area ratio, were approximately 0.13 and 0.18 for the PCL-g-QPDMA-PMA1-REDV and PCL-g-QPDMA-PMA2-REDV surfaces, respectively, indicating the amount of REDV peptides conjugated onto the PCL-g-QPDMA-PMA2 surfaces was higher than that onto the PCL-g-QPDMA-PMA1 surface. In fact, the reactive -COOH of the zwitterionic QPDMA-PMA brushes acted as the anchoring sites for REDV binding, and the grafting density of conjugated REDV peptides was significantly affected by the amount of grafted zwitterionic QPDMA-PMA chains. Therefore, the grafting density of REDV peptides on the PCL-g-QPDMA-PMA2-REDV surface at about $1.43 \pm 0.17 \text{ mg}\cdot\text{cm}^{-2}$ was found to be much larger than that on the PCL-g-QPDMA-PMA2-REDV surface at $0.82 \pm 0.13 \text{ mg}\cdot\text{cm}^{-2}$ (Table 1). This result was further evidence that the surface concentration of -COOH on the QPDMA-PMA chains was positively correlated with the amount of conjugated REDV peptides. The conjugation of REDV peptides onto the zwitterionic QPDMA-PMA-grafted surfaces further improved the surface hydrophilicity, as the static water contact angles decreased to about $33 \pm 2^\circ$ for PCL-g-QPDMA-PMA1-REDV and $24 \pm 3^\circ$ for the PCL-g-QPDMA-PMA2-REDV surfaces (Table 1).

3.5 Determination of antibacterial activities of the functionalized PCL films

The pendant quaternary ammonium groups (N^+) on the zwitterionic polymeric chains are well-known to endow the substrate surfaces with desirable antibacterial functionality to reduce bacterial adhesion.^{51, 52} To determine antibacterial capacity of the functionalized PCL surfaces to kill bacteria upon contact, the LIVE/DEAD[®] two-color fluorescence method and *in vitro* antibacterial assays were performed using Gram-negative *E. coli*. For the waterborne antibacterial assays with fluorescence

microscope (FM) images, the distribution of viable and dead bacterial cells on the pristine and functionalized PCL film surfaces are distinguished by the green (viable) and red (dead) fluorescence staining (Fig. 8 and Supplementary Information, Fig. S6). After 3 h of exposure to the *E. coli* suspension, a large amount of bacterial cells with green fluorescence, either individually or in small clusters, were bestrewed over the pristine PCL surface (Fig. 8a), while only several cells with red fluorescence can be observed for the pristine PCL surface, indicating that most of the bacterial cells were viable with the cell membrane intact on the pristine PCL surface (Fig. 8b). In spite of the improvement in surface hydrophilicity by introducing amine groups or grafting of PDMA-PMA brushes, no significant reduction in the attached bacterial cells can be

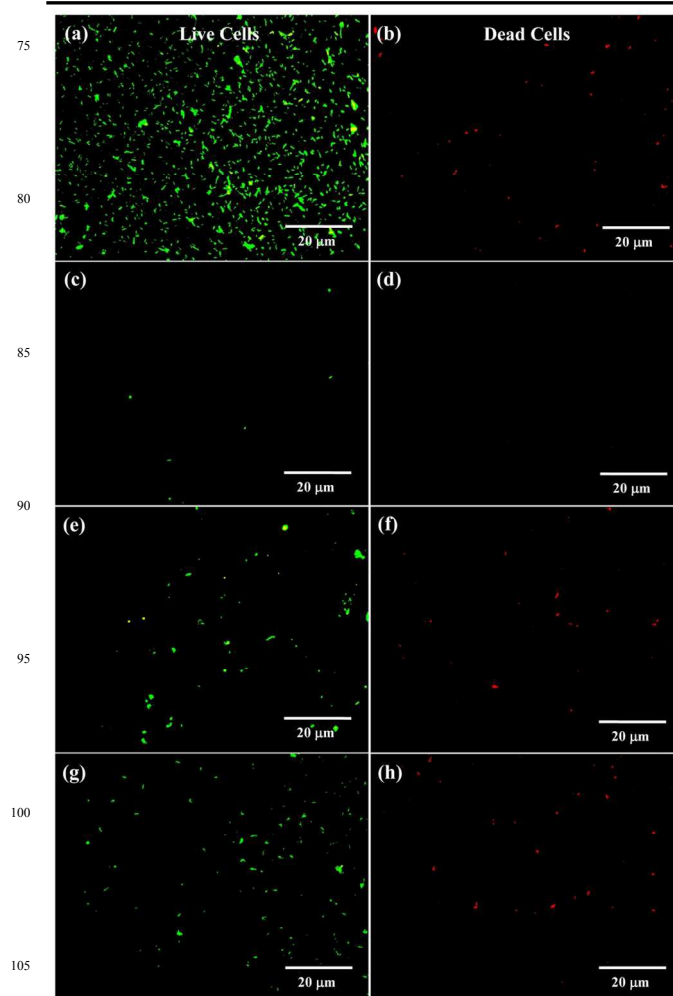


Fig. 8 Representative fluorescence microscopy images of *E. coli* for the (a,b) pristine PCL, (c,d) PCL-g-QPDMA-PMA2, (e,f) PCL-g-QPDMA-PMA1-REDV and (g,h) PCL-g-QPDMA-PMA2-REDV surfaces under the green filter (a,c,e,g) and the red filter (b,d,f,h) after 3 h of exposure in a *E. coli* suspension at a concentration of 1×10^7 cells/mL. The antibacterial activities of the surface-functionalized PCL films with REDV-conjugated zwitterionic polycarboxybetaine brushes were ascertained by the significant decrease in the attached cell number as compared to that on the pristine PCL films.

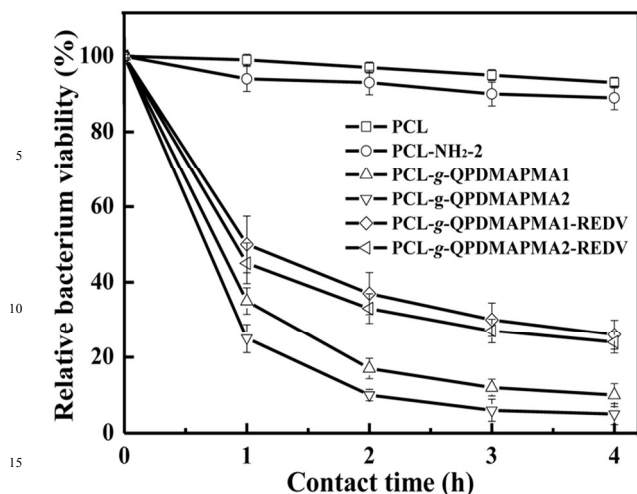


Fig. 9 Survival ratios of viable *E. coli* cells in PBS at 37°C as a function of contact time on different PCL substrates. The cell number was determined by the spread plate method. An approximately 80% decrease in viable cell number demonstrates a high antibacterial efficiency against *E. coli* on the REDV-conjugated PCL film surfaces.

observed on the PCL-NH₂-2 and PCL-g-PDMPMA2 film surfaces (Supporting Information, Figs. S6a-S6d). Many viable cells (stained-green) were spotted to uniformly distribute over the aminolyzed PCL and PDMPMA-grafted surfaces (Figs. S6a and S6c). Taken together, these results are in good agreement with previous findings that the intrinsic hydrophobic PCL surface is favorable template for microorganisms to attach and proliferate for eventually biofilm formation.⁵³

The repeat unit of zwitterionic polycarboxybetaine brushes structurally contains an anionic carboxylic group and a cationic quaternary ammonium groups to endow itself with multifunctionality, such as high resistance to nonspecific adsorption and antibacterial ability.^{25, 52} With the presence of zwitterionic polycarboxybetaine brushes on the PCL film surface, almost no bacterial cells remained distributed over the PCL-g-QPDMAPMA1 (Fig. S6e) and PCL-g-QPDMAPMA2 surfaces (Fig. 8c). The high antibacterial efficiency of QPDMAPMA-grafted PCL surfaces was probably ascribed to the synergistic effect of bactericidal and anti-adhesive capability of zwitterionic polycarboxybetaine brushes. The -COOH groups on the zwitterionic QPDMAPMA chains were able to reduce bacterial adhesion due to the improvement of surface hydrophilicity and resistance to nonspecific adsorption, while the quaternary ammonium compounds on the zwitterionic QPDMAPMA chains killed bacterial cells and conferred bactericidal properties on the PCL surfaces.⁵⁴ Previous studies have reported that dynamic motion of grafted polymeric brushes-type chains could mechanically repel the bacterial adhesion, whilst the polycationic features of brush-like side chains, i.e. quaternary ammonium compounds, affect the antibacterial activity with disrupting ability of bacterial membrane via electrostatic interactions at the time of contact.^{55, 56} Moreover, the antibacterial efficiency of *E. coli* on the

PCL-g-QPDMAPMA2 surface appeared to be higher than that of the PCL-g-QPDMAPMA1 surface, indicating that the antibacterial effect of the functionalized PCL surfaces was positively correlated with the surface concentration of zwitterionic QPDMAPMA brushes. Upon the immobilization of REDV peptides on the QPDMAPMA surfaces, no significant change in the antibacterial capacity was observed, as only several single bacterial cells remained sparsely distributed over the REDV-conjugated QPDMAPMA hybrid surfaces (Figs. 8e and 8g). This result was consistent with the previous findings that the conjugation of biologically-active molecules such as antibodies,⁵⁷ enzymes^{52, 58} and peptides,⁵⁹ to the side chains of zwitterionic polymer brushes has little effect on the nonfouling and antibacterial properties. The current study further confirmed that the REDV immobilized-zwitterionic polycarboxybetaine brushes still remained lethal to bacterial cells on contact, albeit of the slight compromised antibacterial efficiency to Gram-negative *E. coli* bacteria.

To further ascertain the antibacterial efficiency of the REDV-conjugated zwitterionic QPDMAPMA surface in a more quantitative manner, an *in vitro* antibacterial test was also carried, in which the effect of contact time on the killing efficiency of viable *E. coli* cells on the pristine PCL and functionalized PCL film surfaces was investigated. Our results (Fig. 9) showed that the number of viable bacterial cells in the *E. coli* suspension decreased only by less than 10% after 4 h in the contact with the pristine PCL and PCL-NH₂-2 surfaces. This relatively small decrease in bacterial cells may be caused by natural cell death itself. On the other hand, the viable cell number of *E. coli* was found to decrease by more than 70% after 1 h on the zwitterionic QPDMAPMA-grafted PCL surfaces. In fact, more than 90% of viable bacterial cells were killed after 4 h of contact with the zwitterionic QPDMAPMA-grafted surfaces. Moreover, the killing efficiency of *E. coli* on the PCL-g-QPDMAPMA2 surface was higher by about 5% as compared to the PCL-g-QPDMAPMA1 surface. This result demonstrates that the higher the surface density of the quaternary ammonium groups on the side chains of the zwitterionic QPDMAPMA brushes the stronger the antibacterial functionality. In addition, the viable cells in the *E. coli* suspension was found to decrease by more than 50% after 1 h of in contact with the REDV-conjugated QPDMAPMA hybrid surfaces, and around 80% of *E. coli* cells were killed after 4 h of exposure. The result was consistent with the previous observation from cell viability staining (Figs. 8e and 8g) that showed a slight decrease in antibacterial efficacy upon the immobilization of REDV peptides onto the side chains of the zwitterionic QPDMAPMA brushes.

3.6 *In vitro* platelet assays of the functionalized PCL films

Platelets play a crucial role in thrombus formation for the foreign implant surfaces in contact with blood. If the interactions between the implant surfaces and platelets are very weak, the surface will present low platelet adhesion numbers and the adhered platelets maintain their discoid shape with small spreading area.⁶⁰ Thus, platelet spreading

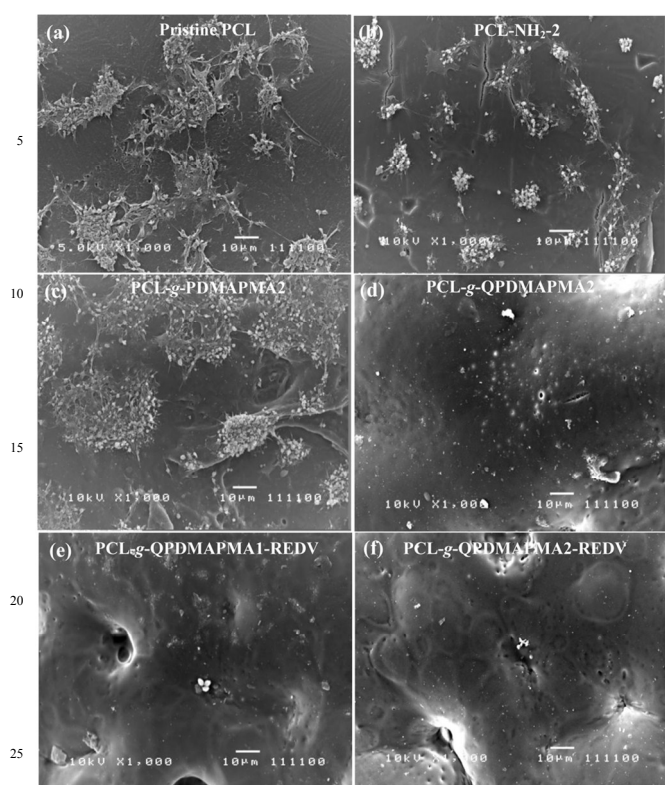


Fig. 10 Representative SEM images of platelet adhesion on the (a) pristine PCL, (b) PCL-NH₂-2, (c) PCL-g-PDMAPMA2, (d) PCL-g-QPDMAPMA2, (e) PCL-g-QPDMAPMA1-REDV, and PCL-g-QPDMAPMA2-REDV surfaces after 90 min incubation with platelet-rich plasma (PRP) at 37°C. The improved hemocompatibility of the PCL film surfaces with REDV-conjugated zwitterionic polycarboxybetaine brushes was demonstrated by the significant reduction in platelet adhesion as compared to that of the PCL surfaces.

and aggregation on the surface are the main factors to evaluate the blood compatibility of biomaterials. Fig. 10 showed the respective SEM images of platelet adhesion on the pristine PCL and functionalized PCL surfaces after *in vitro* contact with PRP for 90 min. Statistically-significant quantitative data was also given in Supporting Information Fig. S7. The relative platelet adhesion was determined by normalizing the number of the attached platelets observed by SEM on each surface by the number of platelets on the pristine PCL surface. As shown in Figs. 10a and 10c, the pristine PCL and PCL-g-PDMAPMA2 surfaces were covered with large areas of spreading platelets. In contrast, the number of attached platelets to both the zwitterionic QPDMAPMA-grafted PCL surface and the REDV-conjugated QPDMAPMA hybrid surfaces was significantly lower than that on the pristine PCL, aminolyzed PCL and PDMAPMA-grafted PCL surfaces (Figs. 10d-10f). In addition, no spreading morphologies can be observed on the PCL-g-QPDMAPMA2 and PCL-g-QPDMAPMA-REDV surfaces. On the other hand, the number of attached platelets on the PCL-g-QPDMAPMA2 surface was more than four times lower than that on the pristine PCL surfaces (Fig. S7). Furthermore, no

significant difference in platelet adhesion can be distinguished between the zwitterionic QPDMAPMA-grafted surfaces and REDV-conjugated QPDMAPMA hybrid surfaces, although the latter surfaces show a slight increase in the number of the attached platelets. Hence, the current results successfully demonstrated that the resistance of the functionalized PCL surface to platelet adhesion was derived from the surface-grafted zwitterionic polycarboxybetaine brushes rather than from the conjugated REDV short peptides. This finding was well consistent with the previous findings that REDV peptide by itself has no inhibition effect on platelet binding.⁶¹ The zwitterionic polycarboxybetaine brushes have been found to hinder the fibrinogen adsorption on substrate surface by the electrostatic repulsion between the negatively-charged carboxyl groups and the net negative charge of fibrinogen in blood plasma, thus inhibiting the fibrinogen-induced platelet activation and subsequent thrombotic responses.²⁶

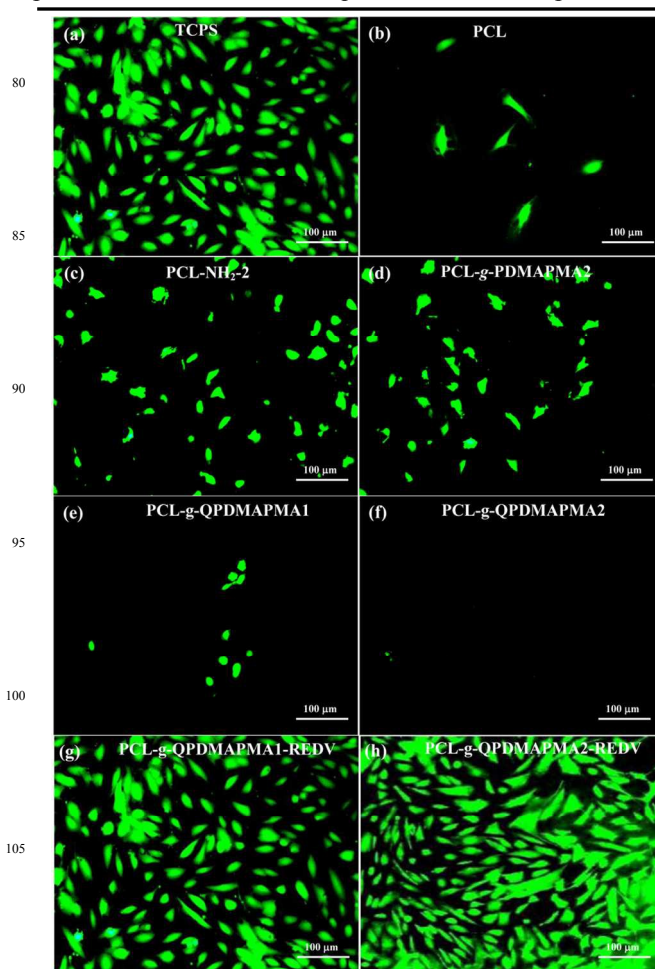


Fig. 11 Fluorescence images of LIVE/DEAD-stained ECs on the (a) TCPS, (b) pristine PCL, (c) PCL-NH₂-2, (d) PCL-g-PDMAPMA2, (e) PCL-g-QPDMAPMA1, (f) PCL-g-QPDMAPMA2, (g) PCL-g-QPDMAPMA1-REDV and (h) PCL-g-QPDMAPMA2-REDV surfaces after 7 days of cell culture. Viable cells emit a green fluorescence, whilst dead cells emit a red fluorescence. Scale bar: 100 μm. A confluent layer of viable cells was observed over the REDV-immobilized PCL substrates.

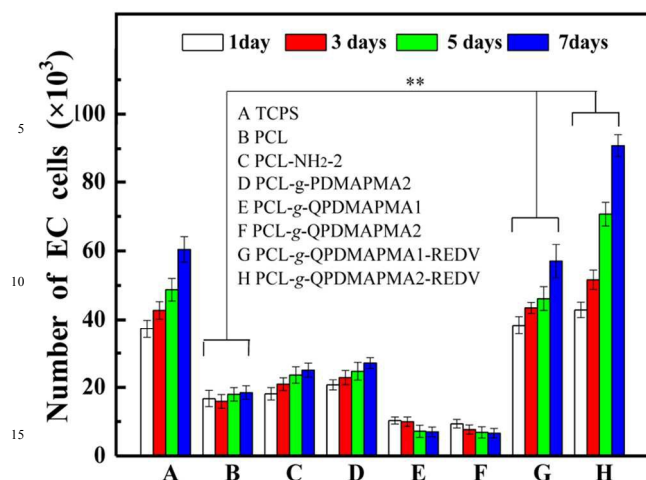


Figure 12 Cell proliferation profiles for the HUVECs on the pristine PCL and surface-functionalized PCL surfaces after 1, 20 3, 5 and 7 days of incubation at 37°C in a 5% CO₂ atmosphere as determined by the AlamarBlue assay. Tissue culture plate (TCPS) was used as a control. * $p < 0.05$ and ** $p < 0.01$ refer to the statistically significant difference compared with the pristine PCL. Significant improvement of the attachment and 25 growth of EC was found on the REDV-immobilized PCL substrates.

3.7 EC adhesion and proliferation on the functionalized PCL film surfaces

3.7.1 EC adhesion and surface endothelialization

The HUVEC adhesion and coverage on the functionalized PCL films, as visualized by nuclear DPAI- and LIVE/DEAD[®]-staining, provided a good assessment of the extent of endothelialization on the surfaces, as well as 35 cell morphology and population doublings rate of the ECs on each substrate (Fig. 11). EC coverage over the course of 7 days was largely determined by initial attachment (Supporting Information, Fig. S8), and cumulative population doublings. In fact, poor support for initial attachment of ECs was evident on the pristine PCL, aminolyzed PCL-NH₂-2 and PCL-g-PDMPMA2 surfaces (Fig. S8b). The sparsely populated ECs on the pristine PCL surfaces was consistent with previous findings that the inherent hydrophobicity and lack of biological recognition 40 sites for PCL made it unfavorable for cell attachment and growth (Fig. 11b).⁶² The PCL-NH₂-2 and PCL-g-PDMPMA2 surfaces resulted in a slightly better coverage of ECs due to the improvement in initial attachment, but the EC growing on these surfaces had irregular morphologies (Figs. 11c and 11d). The least coverage was observed on the zwitterionic QPDMAPMA-grafted surfaces, which was consistent with poor support of the EC attachment and population doublings on the zwitterionic polycarboxybetaine surfaces (Figs 11e and 50 11f). In particular, almost no ECs were present on the PCL-g-QPDMAPMA2 surface (Fig. 11f). However, the ECs on the REDV-immobilized PCL film surfaces were well spread and dense, and the entire surfaces of the

REDV-immobilized PCL surfaces were covered with a 60 confluent layer of ECs (Figs. 11g and 11h), indicating substantially improved endothelialization of the substrate surfaces. Moreover, since the PCL-g-QPDMAPMA2-REDV surface exhibited a better coverage of ECs than the PCL-g-QPDMAPMA1-REDV surface, the extent of 65 endothelialization was also found to be positively correlated with the surface density of the immobilized REDV peptides. Interestingly, apart from REDV-immobilized surfaces, the other surfaces exhibited similar cumulative population doublings on day 7 to the attached cell amount after 24 h, indicating that cell division did not contribute much on most of the surfaces, and it was initial attachment which played a more important role. Taken together, the immobilization of REDV peptides onto the zwitterionic polycarboxybetaine brushes provided specific 75 biological cues to promote better adhesion and endothelialization by the ECs as compared to the pristine PCL or the bare zwitterionic polycarboxybetaine-grafted PCL surfaces.

3.7.2 Cell proliferation

The viability and proliferation of HUVECs on the functionalized PCL surface were quantitatively evaluated by the AlamarBlue[™] (AB) assay, and the results were shown in Fig. 12. The least conducive surface for the EC growth was observed to be that of the pristine PCL film 85 surface. The inherent hydrophobicity and lack of biological cues on the pristine PCL surfaces account for the poor adhesion and proliferation of ECs on the pristine PCL films. Only slight improvement in the EC growth was observed on the PCL-NH₂-2 and PDMPMA-grafted 90 surfaces, in spite of the evident improvement in hydrophilicity of these two surfaces over the pristine PCL surfaces (Table 1). Furthermore, poor support for the EC adhesion and growth was evident on the zwitterionic QPDMAPMA-grafted surfaces, which was in good agreement with previous findings that the ability of the zwitterionic polycarboxybetaine brushes to resist nonspecific adhesion is unfavorable to the attachment and growth of cells.⁶³ In particular, the previous studies have reported that the high flexibility of the hydrophilic 100 zwitterionic polycarboxybetaine chains can retard the cell approaching to the substrate surfaces, thus leading to an unfavorable surface for cell anchorage, in spite of the presence of hydrophilic groups such as -OH and -COOH.⁴⁶ However, upon the immobilization of the REDV short peptides onto the zwitterionic QPDMAPMA chains, the attachment and growth of ECs were significantly improved as a result of the positive cell-material interactions from the immobilized bioactive REDV peptide motifs, leading to overall greater proliferation throughout 105 the course of 7 days than the other functionalized PCL surfaces. In fact, the EC population doublings on the PCL-g-QPDMAPMA1-REDV and PCL-g-QPDMAPMA2-REDV surfaces were comparable to that of the tissue culture polystyrene (i.e. TCPS) positive control. Also, the 115 EC proliferation rate was found to be positively correlated with surface density of the immobilized REDV peptides,

since the cell numbers on the PCL-g-QPDMAPMA2-REDV surfaces with a REDV concentration of $1.43 \pm 0.17 \text{ mg}\cdot\text{cm}^{-2}$ was much higher than that of the PCL-g-QPDMAPMA1-REDV surfaces with a REDV concentration of $0.82 \pm 0.13 \text{ mg}\cdot\text{cm}^{-2}$. Overall, the REDV-conjugated zwitterionic polycarboxybetaine hybrid surfaces exhibit an obvious improvement in the attachment and growth of HUVECs due to the growth-promoting property of the REDV short peptides.

4. Conclusion

A novel multifunctional PCL surface with antibacterial, anti-thrombogenic and cytocompatible properties was designed by the covalent immobilization of REDV peptide onto zwitterionic polycarboxybetaine chains. The synergistic effect of zwitterionic polycarboxybetaine and bioactive REDV peptides was achieved by stepwise grafting of the REDV molecules onto the PCL surfaces. The formation of zwitterionic polycarboxybetaine brushes was accomplished by the combination of surface-initiated ATRP of DMAPMA and subsequent *N*-alkylation of the tertiary amino groups on the PDMAPMA chains with chloroacetates. The pendant carboxyl groups of zwitterionic QPDMAPMA brushes were used for direct conjugation of specific cell-adhesive REDV peptides via carbodiimide reaction. The grafting density of zwitterionic polycarboxybetaine chains and the immobilized REDV peptides were found to be readily modulated by varying surface density of the initiator and the polymerization time. The as-synthesized REDV-QPDMAPMA hybrid surfaces exhibited improved bactericidal and hemocompatible properties as compared to the pristine PCL surfaces, and the immobilization of REDV peptides did not significantly compromise the bactericidal and antifouling activities of zwitterionic polymer brushes, but instead, promoted the adhesion and proliferation of ECs. Overall, the use of the current multifunctional PCL surface for engineering vascular scaffolds is a promising approach, since it allows for improved endothelialization, bactericidal and hemocompatibility.

Associated content

Supporting Information. The ATR-FTIR and XPS spectra of the pristine PCL and aminolyzed PCL-NH₂ surface from aminolysis treatment (Figs. S1 and S2), XPS spectra of the PCL-Br surface (Fig. S3), grafting kinetic curves of PDMADMA brushes as a function of reaction time (Fig. S4), ATR-FTIR spectra of the zwitterionic QPDMAPMA-grafted surfaces (Fig. S5), fluorescence images of *E. coli* attached on different substrates after 3 h of incubation (Fig. S6), platelet adhesion curve (Fig. S7) and fluorescence images of DAPI-staining of ECs attached to different substrate surfaces (Fig. S8).

Acknowledgment

The authors would like to acknowledge the financial assistance of key project of National Natural Science Foundation of China (NO. 21236004).

Notes and references

1. M. B. Gorbet and M. V. Sefton, *Biomaterials*, 2004, **25**, 5681-5703.
2. S. Sarkar, T. Schmitz-Rixen, G. Hamilton and A. M. Seifalian, *Med. Biol. Eng. Comput.*, 2007, **45**, 327-336.
3. D. W. Losordo, J. M. Isner and L. J. Diaz-Sandoval, *Circulation*, 2003, **107**, 2635-2637.
4. A. V. Finn, M. Joner, G. Nakazawa, F. Kolodgie, J. Newell, M. C. John, H. K. Gold and R. Virmani, *Circulation*, 2007, **115**, 2435-2441.
5. C. K. Poh, Z. Shi, T. Y. Lim, K. G. Neoh and W. Wang, *Biomaterials*, 2010, **31**, 1578-1585.
6. Y. Liu, T. T. Y. Tan, S. J. Yuan and C. Choong, *J. Mater. Chem. B*, 2013, **1**, 157-167.
7. O. Leroy, A. Meybeck, B. Sarraz-Bournet, P. d'Elia, L. Legout, *Curr. Opin. Infect. Dis.* 2012, **25**, 154-158.
8. L. L. Pounds, M. Montes-Walters, C. G. Mayhall, P. S. Falk, E. Sanderson, G. C. Hunter and L. A. Killewich, *Vasc. Endovasc. Surg.* 2005, **39**, T1-T7.
9. A. Song, A. A. Rane and K. L. Christman, *Acta Biomater.* 2012, **8**, 41-50.
10. P. H. Chua, K. G. Neoh, Z. Shi and E. T. Kang, *J. Biomed. Mater. Res. Part A* 2008, **87**, 1061-1074.
11. B. Guo and P. X. Ma, *Sci. China Chem.* 2014, **57**, 490-500.
12. M. A. Woodruff and D. W. Huttmacher, *Prog. Polym. Sci.* 2010, **35**, 1217-1256.
13. F. Darain, W. Y. Chan and K. S. Chian, *Soft Mater.* 2010, **9**, 64-78.
14. Z. Ma, C. Gao, J. Yuan, J. Ji, Y. Gong and J. Shen, *J. Appl. Polym. Sci.* 2002, **85**, 2163-2171.
15. E. D. Yildirim, R. Besunder, D. Pappas, F. Allen, S. Güçeri and W. Sun, *Biofabrication*, 2010, **2**, 014109.
16. Y. M. Shin, K.-S. Kim, Y. M. Lim, Y. C. Nho and H. Shin, *Biomacromolecules*, 2008, **9**, 1772-1781.
17. A. Olivier, F. Meyer, J.-M. Raquez, P. Damman and P. Dubois, *Prog. Polym. Sci.* 2012, **37**, 157-181.
18. S. Edmondson, V. L. Osborne and W. T. Huck, *Chem. Soc. Rev.*, 2004, **33**, 14-22.
19. J. S. Wang and K. Matyjaszewski, *J. Am. Chem. Soc.* 1995, **117**, 5614-5615.
20. K. Matyjaszewski and J. Xia, *Chem. Rev.* 2001, **101**, 2921-2990.
21. S. Chen, S. Chen, S. Jiang, Y. Mo, J. Luo, J. Tang and Z. Ge, *Colloid Surface B* 2011, **85**, 323-329.
22. H. Jiang and F. J. Xu, *Chem. Soc. Rev.* 2013, **42**, 3394-3426.
23. W. Yuan, C. Li, C. Zhao, C. Sui, W. Yang, F. Xu and J. Ma, *Adv. Funct. Mater.* 2012, **22**, 1835-1842.
24. Y. Hu, N. Zhao, J. Li, W. Yang and F. Xu, *J. Mater. Chem.* 2012, **22**, 21257-21264.
25. F. Xu, Z. Wang and W. Yang, *Biomaterials*, 2010, **31**, 3139-3147.
26. L. Mi and S. Jiang, *Biomaterials*, 2012, **33**, 8928-8933.
27. H. Jiang, X. Wang, C. Li, J. Li, F. Xu, C. Mao, W. Yang and J. Shen, *Langmuir*, 2011, **27**, 11575-11581.
28. Y. Chang, W. J. Chang, Y. J. Shih, T. C. Wei and G. H. Hsiue, *ACS Appl. Mater. Interf.* 2011, **3**, 1228-1237.
29. Y. Ji, Y. Wei, X. Liu, J. Wang, K. Ren and J. Ji, *J. Biomed. Mater. Res. Part A* 2012, **100**, 1387-1397.
30. J. A. Hubbell, S. P. Massia, N. P. Desai and P. D. Drumheller, *Nat. Biotechnol.* 1991, **9**, 568-572.
31. M. Yanagisawa, H. Kurihara, S. Kimura, Y. Tomobe, M. Kobayashi, Y. Mitsui, Y. Yazaki, K. Goto and T. Masaki, *Nature*, 1988, **332**, 411-415.
32. S. Massia and J. Hubbell, *J. Biol. Chem.* 1992, **267**, 14019-14026.
33. Z. Y. Yang, S. J. Yuan, B. Liang, Y. Liu and C. Choong, *Macromol. Biosci.* 2011, **14**, 1299-1311.
34. H. Zhang, C. Y. Lin and S. J. Hollister, *Biomaterials*, 2009, **30**, 4063-4069.
35. S. J. Yuan, G. Xiong, A. Roguin and C. Choong, *Biointerphases*, 2012, **7**, 30.
36. A. B. Lowe and C. L. McCormick, *Chem. Rev.* 2002, **102**, 4177-4190.
37. Y. M. Shin, K.-S. Kim, Y. M. Lim, Y. C. Nho and H. Shin, *Biomacromolecules*, 2008, **9**, 1772-1781.
38. J. S. Bae, E. J. Seo and I. K. Kang, *Biomaterials*, 1999, **20**, 529-537.
39. S. J. Yuan and S. Pehkonen, *Colloid Surface B* 2007, **59**, 87-99.
40. Y. H. Kim, M. A. Jyoti and H. Y. Song, *Appl. Surf. Sci.* 2014, **303**, 97-106.

41. M. Sahebalzamani and E. Biazar, *J. Biomater. Tiss. Eng.* 2014, **4**, 423-429.
42. M. Ansari, S. Salahshour-Kordestani, M. Habibi-Rezaei and A. A. M. Movahedi, *J. Macromol. Sci. B* 2015, **54**, 71-80.
- 5 43. J. F. Moulder, J. Chastain and R. C. King, *Handbook of X-ray Photoelectron Spectroscopy*. Perkin-Elmer Eden Prairie, MN, 1992.
44. Y. Xia, F. Boey and S. S. Venkatraman, *Biointerphases*, 2010, **5**, FA32-FA40.
45. A. Das and A. R. Ray, *J. Appl. Polym. Sci.* 2008, **108**, 1273-1280.
- 10 46. T. Ren, S. Yu, Z. Mao and C. Gao, *Biomaterials*, 2015, **56**, 58-67.
47. Y. Liu, L. Wang and C. Pan, *Macromolecules*, 1999, **32**, 8301-8305.
48. S. J. Yuan, G. Xiong, X. Wang, S. Zhang and C. Choong, *J. Mater. Chem.* 2012, **22**, 13039-13049.
49. G. Zhai, Z. L. Shi, E. T. Kang and K. G. Neoh, *Macromol. Biosci.* 15 2005, **5**, 974-982.
50. L. Zhang, H. Xue, C. Gao, L. Carr, J. Wang, B. Chu and S. Jiang, *Biomaterials*, 2010, **31**, 6582-6588.
51. R. Lalani and L. Liu, *Biomacromolecules*, 2012, **13**, 1853-1863.
52. G. Cheng, G. Li, H. Xue, S. Chen, J. D. Bryers and S. Jiang, 20 2009, **30**, 5234-5240.
53. A. R. Sarasam, R. K. Krishnaswamy and S. V. Madihally, *Biomacromolecules*, 2006, **7**, 1131-1138.
54. T. J. Franklin, G. A. Snow, *Biochemistry of antimicrobial action*, Chapman & Hall LTD, London, 1981
- 25 55. S. Buffet-Bataillon, P. Tattevin, M. Bonnaure-Mallet and A. Jolivet-Gougeon, *Int. J. Antimicrobi. Ag.* 2012, **39**, 381-389.
56. M. Gultekinoglu, Y. Tunc Sarisozen, C. Erdogdu, M. Sagiroglu, E. A. Aksoy, Y. J. Oh, P. Hinterdorfer and K. Ulubayram, *Acta Biomater.* 2015, **21**, 44-54.
- 30 57. G. Kim, C. E. Yoo, M. Kim, H. J. Kang, D. Park, M. Lee and N. Huh, *Bioconjugate Chem.* 2012, **23**, 2114-2120.
58. Z. Zhang, S. Chen and S. Jiang, *Biomacromolecules*, 2006, **7**, 3311-3315.
59. Q. Li, Z. Wang, S. Zhang, W. Zheng, Q. Zhao, J. Zhang, L. Wang, S. Wang and D. Kong, *Mat. Sci. Engi. C-Mater.* 2013, **33**, 1646-1653.
- 35 60. M. Kanno, H. Kawakami, S. Nagaoka and S. Kubota, *J. Biomed. Mater. Res.* 2002, **60**, 53-60.
61. H. Ceylan, A. B. Tekinay and M. O. Guler, *Biomaterials*, 2011, **32**, 8797-8805.
- 40 62. T. Jacobs, H. Declercq, N. De Geyter, R. Cornelissen, P. Dubruel, C. Leys and R. Morent, *Surf. Coat. Technol.* 2013, **232**, 447-455.
63. H. W. Chien, C. C. Tsai, W. B. Tsai, M.-J. Wang, W. H. Kuo, T. C. Wei and S. T. Huang, *Colloid Surface B* 2013, **107**, 152-159.

TOC Graphic

Title: Multifunctional REDV-conjugated zwitterionic polycarboxybetaine-polycaprolactone hybrid surfaces for enhanced antibacterial activity, antithrombogenicity and endothelial cell proliferation

Authors: Shaojun Yuan,^{a,*} Gorden Xiong,^b Fei He,^a Wei Jiang,^a Bin Liang,^a and Cleo Choong^{b,*}

Multifunctional polycaprolactone (PCL) hybrid surfaces are developed by grafting of REDV-zwitterionic polycarboxybetaine conjugates via surface-initiated atom transfer radical polymerization (ATRP). The as-synthesized surfaces exhibit high efficiency to kill bacteria on contact and to resist platelet adhesion, whilst simultaneously promotes the adhesion and proliferation of human umbilical vein endothelial cells (HUVECs).

